Geomechanics and Engineering, *Vol. 5, No. 3 (2013) 241-261*
DOI: http://dx.doi.org/10.12989/gae.2013.5.3.241

Numerical study on bearing behavior of pile considering sand particle crushing

Yang Wu*[1], Haruyuki Yamamoto[1a] and Yangping Yao[2b]

[1]*Graduate School for International Development and Cooperation, Hiroshima University, Higashi-Hiroshima 739-8529, Japan*
[2]*Department of Civil Engineering, Beihang University, Beijing 100191, China*

(Received August 30, 2012, Revised February 19, 2013, Accepted March 20, 2013)

Abstract. The bearing mechanism of pile during installation and loading process which controls the deformation and distribution of strain and stress in the soil surrounding pile tip is complex and full of much uncertainty. It is pointed out that particle crushing occurs in significant stress concentrated region such as the area surrounding pile tip. The solution to this problem requires the understanding and modeling of the mechanical behavior of granular soil under high pressures. This study aims to investigate the sand behavior around pile tip considering the characteristics of sand crushing. The numerical analysis of model pile loading test under different surcharge pressure with constitutive model for sand crushing is presented. This constitutive model is capable of predicting the dilatancy of soil from negative to positive under low confining pressure and only negative dilatancy under high confining pressure. The predicted relationships between the normalized bearing stress and normalized displacement are agreeable with the experimental results during the entire loading process. It is estimated from numerical results that the vertical stress beneath pile tip is up to 20 MPa which is large enough to cause sand to be crushed. The predicted distribution area of volumetric strain represents that the distributed area shaped wedge for volumetric contraction is beneath pile tip and distributed area for volumetric expansion is near the pile shaft. It is demonstrated that the finite element formulation incorporating a constitutive model for sand with crushing is capable of producing reasonable results for the pile loading problem.

Keywords: constitutive model; particle crushing; finite element analysis; pile foundation; surcharge pressure

1. Introduction

In nature, soil is composed of granular particles and displays dilatancy characteristics when it is subjected to shear stress. The volume changes because of the granular particles rearrangement and compression respectively. It is well known that sand particles show the tendency of being crushed under high-level compressive stress. Particle crushing phenomena of soil was observed by Fukumoto (1992), Lade *et al*. (1996), Mahmoud *et al*. (2008) from a series of compression and

*Corresponding author, Ph.D. Student, E-mail: yangwuuu0226@hotmail.com
[a]Professor, E-mail: a040564@hiroshima-u.ac.jp
[b]Professor, E-mail: y-pyao@buaa.edu.cn

http://www.techno-press.org/?journal=gae&subpage=7 ISSN: 2005-307X (Print), 2092-6219 (Online)

shear experiments. Particle crushing is an irreversible process accompanying with the reduction of strength and dilatancy degree. It was pointed out by Hardin (1985) that the characteristics of particle crushing were determined by many factors, such as the distribution of particle size, stress level and stress path, particle shape and hardness, etc. The effect of the particle crushing on the peak strength of sand is dependent on the confining pressure level not only in the triaxial test but also in engineering practice. In addition, the failure of particle crushing also occurs in significant stress concentrated region such as the area surrounding the pile tip. The bearing capacity of pile is inevitably influenced when sand around the pile tip is compressed and sheared to be crushed.

Plenty of research results on the relationship between the particle crushing phenomena of sand and bearing capacity of pile in sand as well as behavior of sand surrounding pile tip have been acquired. To investigate the stress-strain characteristics of sand in the particle-crushing region, a few of triaxial tests including multi-step stress path test were carried out on Toyoura sand using high-pressure triaxial compression apparatus. Miura *et al*. (1984) established and proposed a new excellent energy expression to improve the prediction correctness of the Modified Cam-clay model. The predicted values showed good agreement with test results. However, the model had no capability of describing sand positive dilatancy under relative low confining pressure. It was presented and concluded by Simonini (1996) about the behavior of dense sand around non-displacement pile tip in the particle-crushing region which was modeled by finite element method. Two important factors: relative density and mean effective stress level were revealed to influence sand particle crushing. Frictional angle was elected as strength parameter in the model. The amount of particle crushing was controlled by complicated function g, in which the relative breakage index B_r was employed. The frictional angle and relative breakage index distribution that indicated the amount of grain crushing at failure around pile tip were reasonably predicted and displayed. Yasufuku and Hyde (1995), Yasufuku *et al*. (2001) also discussed the relationship between the bearing capacity of pile and the load-displacement curve in sand considering the compressibility. The predicted bearing capacity of non-displacement pile in sand based on pile cavity expansion theory was discussed in terms of compressibility factor, friction angle, average volumetric strain and shear stiffness.

The significance of particle crushing on the expression of constitutive relationship and its influence on pile bearing capacity has been realized. Previous researches just link the particle crushing with the estimation formulation for calculating pile bearing capacity or display the distribution of sand strength parameter around the pile tip. Limited numerical study on pile loading or jacking into sand simulated by the constitutive model with the ability of describing the sand crushing behavior has been accomplished.

The aim of this study is to investigate the mechanical behavior of sand surrounding model pile tip in consideration of the volume variant and strength reduction. Further understanding about pile behavior in sand can be achieved by powerful numerical analysis. It is necessary to establish a reasonable constitutive model for sand with the capacity of describing the mechanical behavior even though particle crushing occurs. The constitutive model specified in this study is capable of representing the dilatancy behavior of sand under different confining pressure. This simple constitutive model can describe the peak strength reduction and volume variant in accompany with particle crushing occurrence. In addition, this constitutive model for sand with crushing is simply computation application. Therefore, it is positively employed in numerical analysis.

The numerical analysis of model pile loading test under different surcharge pressure is presented in this study. The major work in numerical analysis is to apply the constitutive model with crushing to represent the behavior of sand. Moreover, in order to apply this simple

constitutive model to practical engineering using FEM, its elasto-plastic constitutive tensor is derived in detail. The predicted results are compared with the experimental results of the model pile loading test in laboratory. The figures for the distributions of stress and strain around the pile tip are displayed under various surcharge pressures and displacements. Developments of the stress and strain contour around the pile tip are similarly beneficial for deeply understanding the pile bearing mechanism.

2. Outline of model pile loading test

In the model pile loading tests conducted by Yamamoto *et al*. (2003), the model piles were jacked into the ground tank container which is filled with Toyoura sand in order to demonstrate the effects of pile tip shape and surcharge pressure level on the bearing capacity, and to study the movement of sand particles around the pile tip area. The testing apparatus is shown in Fig. 1 which consists of the ground tank container, loading installation and measurement part.

The ground tank container is 550 mm in height and 584.2 mm in diameter. The diameters of steel model pile are adopted as 30 mm and 54 mm respectively in Fig. 2. The diameter ratio of the ground tank container to steel model pile is deliberately adjusted to weaken the reaction from the interior surface of the ground tank container. Toyoura sand is poured into the ground tank container layer by layer to be well-distributed and homogeneous after model pile is installed in previous. The relative density of the dense uniform Toyoura sand is approximately 90%. The physical and material parameters of Toyoura sand are listed in detail in Table 1. In addition, the influence of pile installation on bearing capacity is neglected. Teflon sheets and silicon-grease are pasted on the interface between the ground tank container and Toyoura sand to eliminate the effect of fictional stress.

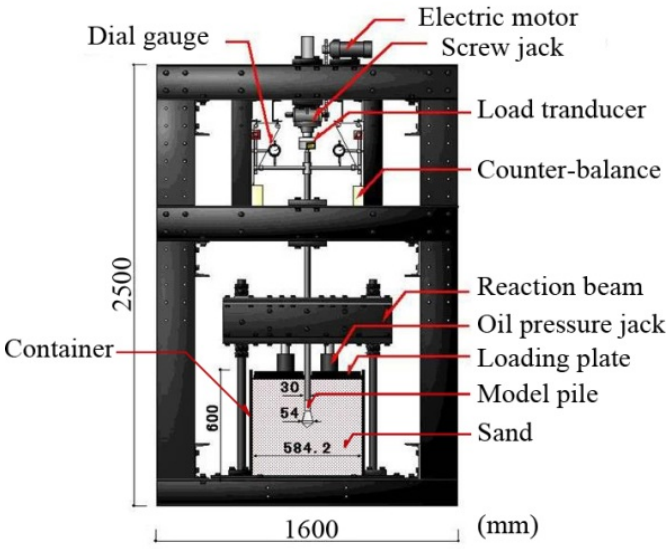

Fig. 1 The testing apparatus

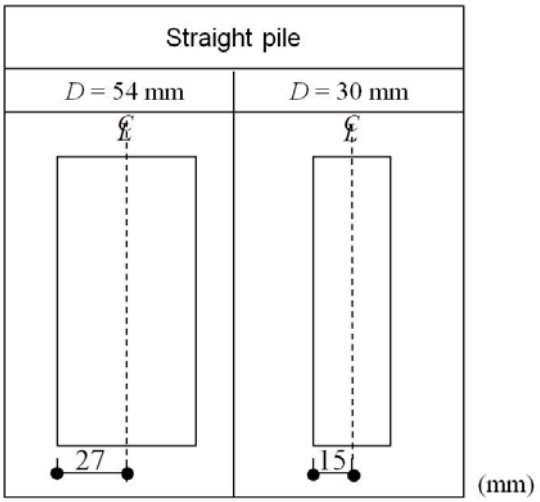

Fig. 2 The model pile with diameters of 30 mm and 54 mm

The model pile loading test is performed with displacement-controlled method. The descending speed of the model pile into sand layer is 0.5 mm/min. The final displacement of the model pile is equal to its diameter. The loading transforms into the sand layer and simulates the actual soil stress underground. Three levels of surcharge pressures 200 kPa, 400 kPa and 600 kPa simulate the actual soil stresses at different depths.

In order to confirm the occurrence of particle crushing in the test, the grain size distribution curves for the Toyoura sand before and after model pile loading test are measured by Li and Yamamoto (2005) in Fig. 3. The part of sand ground for sieve analysis test is a cube column with a pile diameter equal to the side length just beneath the pile tip. The intact sample of sand block is carefully taken off after test completion. The characteristics of the model ground material and the axi-symmetric loading conditions of Li's experiment are identical to the current study. As of the above reasons, the figure is directly cited to prove particle crushing occurrence. As shown in Fig. 3, sand particle become finer with larger surcharge pressure. Before test, the sand particle passing sieve diameter 0.1 mm is less than 5%, however, the percent of sand particle passing 0.1 mm is nearly 15% after tests at the surcharge pressure of 100 kPa and 200 kPa. Particle crushing of soil definitely occurs at the area surrounding the pile tip.

3. Constitutive model considering particle crushing

In recent decade, Daouadji *et al*. (2001) and Daouadji and Hicher (2010) proposed a constitutive model for sand and its enhanced version taking particle breakage into account in which the grain distribution was chosen as the parameter and proved its new theory on the basis of laboratory tests. Kikumoto *et al*. (2010) also discussed the behavior of sand crushing with the revised SEVERN-TRENT sand model choosing a grade state index to consider the changing particle size distribution. The Modified Cam-clay model is originally developed to represent the behavior of normally consolidated clay. Following the same modeling theory, many researchers

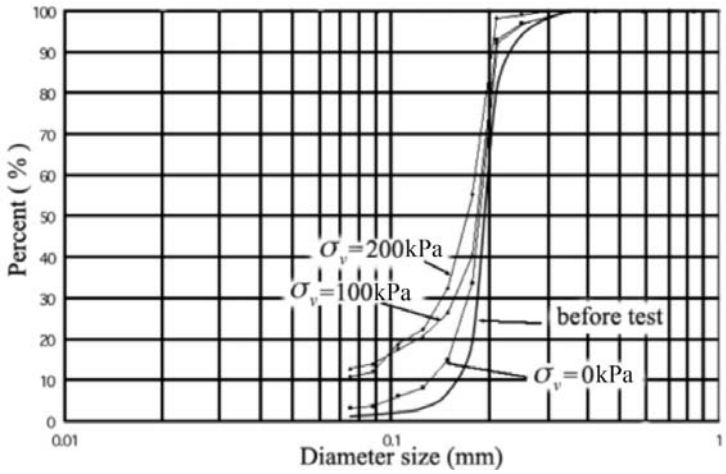

Fig. 3 Distribution curves of sand grain size

attempted to apply it to describe the granular materials like sand. Yao *et al*. (2008b) revised the unified model by introducing the reference crushing stress p_c to establish a model for sand with crushing. This new hardening parameter was capable of predicting the dilatancy behavior of soil from negative to positive under low confining pressure and only negative dilatancy under high confining pressure. This constitutive model is proposed on the basis of critical state theory. It describes the mechanical behavior of sand in macroscopic and not focuses on micro-structure and micro-crack of particle crushing. The validity of model had been verified by the results of triaxial compression on Toyoura sand. Here, the model for sand with crushing is briefly introduced.

3.1 Hardening parameter and prediction of dilatancy

A reasonable hardening parameter controlling plastic volume strain plays a significant role to describe the characteristics of dilatancy. The unified hardening parameter H with the plastic work form in Eq. (1) is derived by Yao *et al*. (2008a) in order to be appropriate for both clay and sand. The newly unified hardening parameter for constitutive model for sand with crushing is revised.

Table 1 Properties of Toyoura sand for testing

Mean grain size (mm)	0.20
Coefficient of uniformity	1.21
Specific gravity	2.656
Minimum density (g/cm^3)	1.332
Maximum density (g/cm^3)	1.646
Relative density (%)	90
Internal friction angle	44.0°

$$dH = \frac{M_c^4}{M_f^4}\frac{M_f^4 - \eta^4}{M_c^4 - \eta^4} d\varepsilon_v^p \tag{1}$$

where M_c is the stress ratio at characteristic state, M_f is the stress ratio at shear failure defined in Eqs. (2) and (3) respectively. η means the ratio of deviatoric stress q to the mean stress p.

$$M_c = M\left(\frac{p}{p_c}\right)^n \tag{2}$$

$$M_f = M\left(\frac{p}{p_c}\right)^{-n} \tag{3}$$

where M and p_c are the stress ratio at critical state and the referenced crushing stress. n is the material parameter. These three curves intersect at the point D ($M_c = M = M_f$).

Combining the equation $M_c = q_c / p$ with Eq. (2) gives the specific expression of q_c in Eq. (4) and combining the equation $M_f = q_f / p$ with Eq. (3) gives the expression of q_f in Eq. (5). In Fig. 4, the horizontal axis stands for the mean stress and vertical axis stands for the devatoric stress. The capital letter *AB*, *CD* and *EF* standing for stress paths with different initial confining pressure level are correspondent to the curves in Fig. 5(a), (b) and (c) respectively. It follows the sign convention in soil mechanics; compression is ruled to be positive value.

$$q_c = Mp_c^{-n} p^{1+n} \tag{4}$$

$$q_f = Mp_c^{n} p^{1-n} \tag{5}$$

The dilatancy prediction theory can be explained with the help of plastic volumetric strain increment. Path *AB*: Stress path begins from the point *A* (low confining pressure) in the Fig. 5(a). The characteristic state will not change until it reaches the point *K*. The plastic volumetric strain increment $d\varepsilon_v^p$ is positive in *AK* phase. The value of $d\varepsilon_v^p$ turns to negative later because it is in

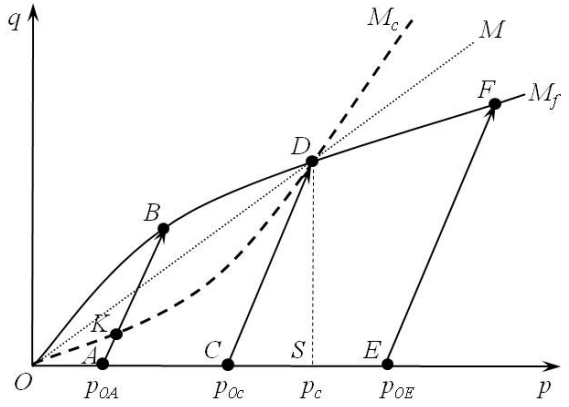

Fig. 4 The curves of M_c and M_f and stress paths in p-q plane

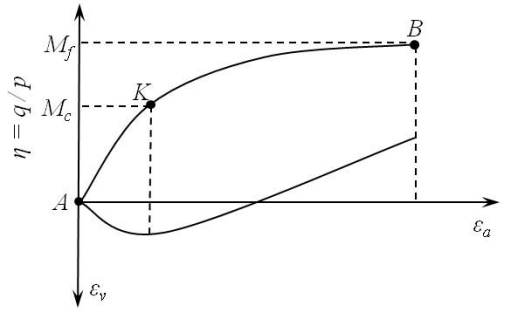

(a) Path *AB*

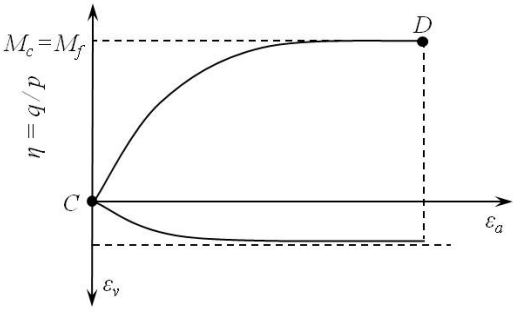

(b) Path *CD*

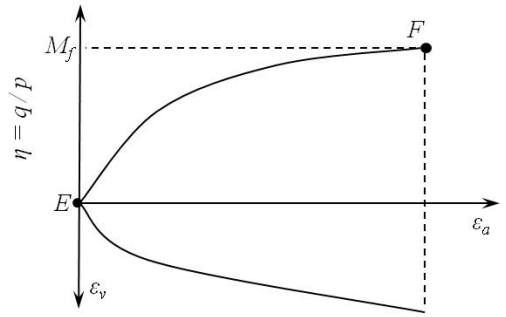

(c) Path *EF*

Fig. 5 The curves of stress-strain relationship at different stress levels

KB phase. We observe the final stage is positive dilatancy. Although in the beginning stage, the curve shows the negative dilatancy. Path *CD*: From Fig. 5(b), the loading path begins from the point *C* (medium confining pressure). The characteristic state changes and failure happens at the same time. The $d\varepsilon_v^p$ is constantly positive value during the entire loading process. The final stage is negative dilatancy. Path *EF*: From Fig. 5(c), the loading path begins from the point *E* (high confining pressure), failure happens before the characteristic state changes because the stress path touches the failure line earlier. The final stage is negative dilatancy.

3.2 Expression and failure criterion of the constitutive model

In the Modified Cam-clay model, the relationships between the elastic and plastic volumetric strain and the logarithm of mean stress ln(p) are expressed in linearity. On the other hand, based on the test results on Toyoura sand, the relationships are derived by the following reasonable power exponential law of mean stress by Nakai (1989).

$$\varepsilon_v^e = C_e\left[\left(\frac{p_x}{p_a}\right)^m - \left(\frac{p_o}{p_a}\right)^m\right] \tag{6}$$

$$\varepsilon_v^p = (C_t - C_e)\left[\left(\frac{p_x}{p_a}\right)^m - \left(\frac{p_o}{p_a}\right)^m\right] \tag{7}$$

where p_o is the initial mean stress, p_a is the atmospheric pressure, C_t is the compression index, C_e is the swelling index and m is a coefficient for sand. p_a takes the value of 0.1 MPa. P_x is the mean stress on horizontal axis in Eqs. (6) and (7). The compression and swelling indexes and material parameter m of the Toyoura sand in a wide range of isotropic stress can be determined by Sun *et al*. (2007).

The stress-dilatacy equation can be expressed as follows

$$\frac{d\varepsilon_v^p}{d\varepsilon_d^p} = \frac{M_c^2 p^2 - q^2}{2pq} \tag{8}$$

The normality condition is shown in Eq. (9)

$$dpd\varepsilon_v^p + dqd\varepsilon_d^p = 0 \tag{9}$$

where $d\varepsilon_d^p$ is the plastic deviatoric stain increment. By combining Eqs. (8) and (9), the yield locus of crushing model is obtained as follows

$$f = (2n+1)\frac{p_c^{2n}}{M^2}\cdot\frac{q^2}{p} + p^{2n+1} - p_x^{2n+1} = 0 \tag{10}$$

In Eq. (10) when n is equal to 0, the yield function is reduced to that of the Modified Cam-clay model. The mean stress p_x at isotropic loading is linked to plastic volumetric strain ε_v^p by Eq. (7). By combining Eqs. (7) and (10), rearranging the expression result and replacing the new revised hardening parameter H, we have

$$f = \frac{C_t - C_e}{p_a^m}\left\{\left[\frac{(2n+1)p_c^{2n}}{M^2}\times\frac{q^2}{p} + p^{2n+1}\right]^{\frac{m}{2n+1}} - p_o^m\right\} - H = 0 \tag{11}$$

Eq. (11) is the yield function of the crushing model. Crushing model takes the associated flow

rule, so that plastic potential function g is identical to yield function f. The plastic strain increment $d\varepsilon_{ij}^{p}$ can be calculated using the flow rule in Eq. (12).

$$d\varepsilon_{ij}^{p} = \Lambda \frac{\partial g}{\partial \sigma_{ij}} \tag{12}$$

where Λ is a scalar, the elastic modulus E varies with the mean stress and is expressed as in Eq. (13)

$$E = \frac{3(1-2v)p_a^m}{mC_e p^{m-1}} \tag{13}$$

where υ is the Poisson ratio and takes value of 0.3 in this study.

3.3 Determination of model parameter

Generally, there are seven parameters in this constitutive model for sand with crushing. Except the Poisson ratio v which is assumed to be 0.3, the other six parameters can be determined via the conventional triaxial compression test. C_e = 0.0016, C_t = 0.0044 and material parameter m = 0.5 are from experiment performed by Sun *et al*. (2007). In Sun's conventional triaxial compression test, specimen of Toyoura sand also adopts the relative density as 90%. Drained triaxial compression test for Toyoura sand at the confining pressure of 0.2 MPa, 0.5 MPa, 1 MPa, 2 MPa, 4 MPa and 8 MPa each are performed. It was found that both the stress ratio q_f / p and the strain increment ratio $d\varepsilon_v / d\varepsilon_a$ becomes constant values when the Toyoura sand is in failure state under different confining pressures. Besides, connecting the points according to failure states in the q_f / p and $d\varepsilon_v / d\varepsilon_a$ plane provides a straight line as shown in Fig. 6. On the linear relation between these two ratio values, the elastic deformation part is ignored. The peak stress ratio is assumed to be equal to M when the volumetric strain increment is zero ($d\varepsilon_v / d\varepsilon_a$ = 0). Utilizing the above linear relationship, we determine M as 1.35 and then make rearrangement of Eq. (3) as in Eq. (14)

$$\ln M_f = -n \ln p + n \ln p_c + \ln M \tag{14}$$

According to the relationship between the curve M_f and the mean stress p in test, we can draw Fig. 7 to express the relationship between ln(M_f) and ln(p), then we get the value of p_c = 5.85 MPa and n = 0.085 respectively. The seven parameters are shown in the Table 2.

3.4 Experiment results and prediction

The triaxial compression test under high confining pressures has a long history. The crushing behavior of dense Toyoura sand with relative density 90% is observed by Miura and Yamanouchi (1971). In Miura's test, confining pressures acting on specimen reach 7.5 MPa and 10 MPa. Recently, a series of triaxial compression tests under high confining pressures are carried out to failure state. Sun's triaxial compression tests were performed with different confining pressures as 0.2 MPa, 0.5 MPa, 1 MPa, 2 MPa, 4 MPa and 8 MPa. The size of the specimen was 100 mm in height and 50 mm in diameter. The relationships between the stress ratio and the axial strain, the volumetric strain and the axial strain, the stress ratio and the radial strain are shown in Figs. 8, 9

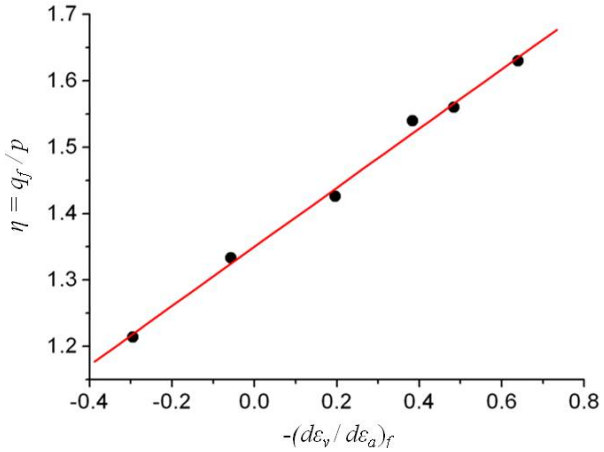

Fig. 6 The relationship between q_f/p and $-(d\varepsilon_v / d\varepsilon_a)_f$ at failure state under different confining pressures

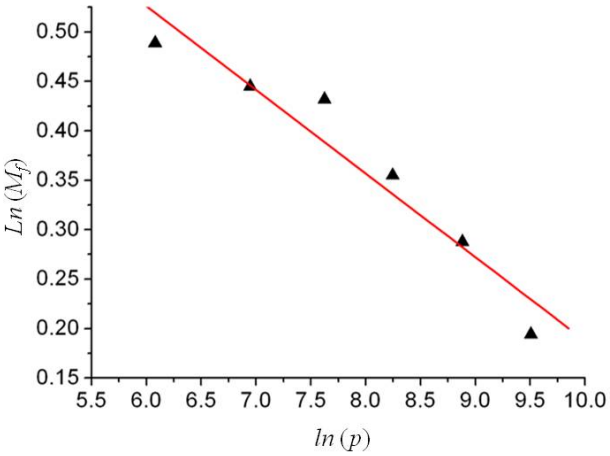

Fig. 7 The relationship between ln(M_f) and ln(p)

Table 2 The seven parameters of the constitutive model for Toyoura sand with crushing

Isotropic consolidation	Triaxial compression	Poisson ratio
$C_e = 0.0016$	$M = 1.35$	
$C_t = 0.0044$	$p_c = 5.85MPa$	$\nu = 0.3$
$m = 0.5$	$n = 0.085$	

and 10. From Fig. 8, we can confirm that stress ratio decreases when the confining pressure increases. In addition, it is observed that the stress ratio remains constant when sand specimen enters into failure with the accumulation of axial strain. The reduction of strength is resulted from the particle crushing. From Fig. 9, we can conclude that sand crushing model can predict dilatancy from negative to positive when the confining pressure is low, at the values of 0.2 MPa, 0.5 MPa, 1 MPa and 2 MPa. It predicts the negative dilatancy when the confining pressure is 4 MPa and 8

MPa. The sharp volumetric reduction of the specimen is attributed to particle crushing. The predicted volume of the sand specimen agrees with the test results expect when confining pressure is 8 MPa. In Fig. 10, the curves variation tendency is similar to these in Fig. 8. Stress ratio becomes almost a constant value after failure state happens.

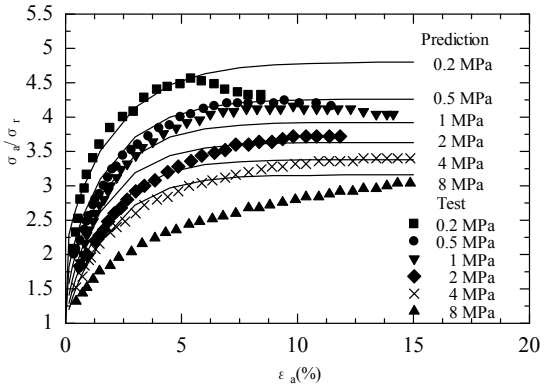

Fig. 8 Relationship between the stress ratio and axial strain

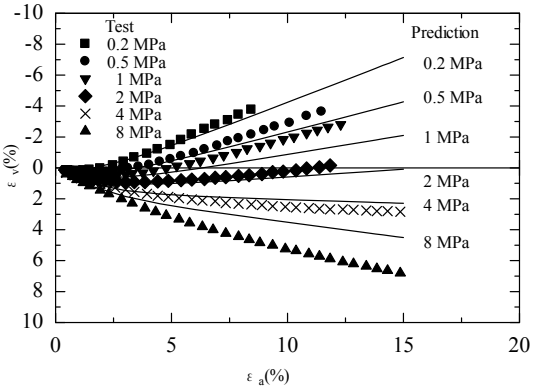

Fig. 9 Relationship between the volumetric strain and axial strain

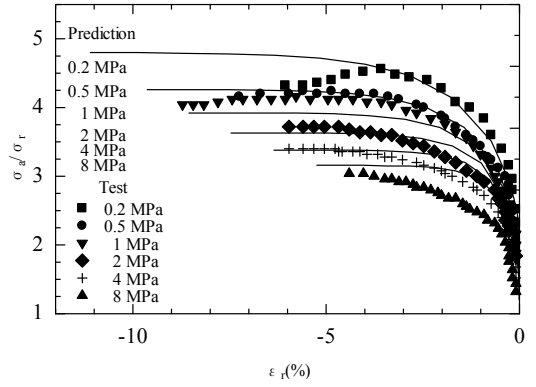

Fig. 10 Relationship between the stress ratio and radial strain

In summary, this simple constitutive model with particle crushing can well describe volumetric change of sand during shear before and after crushing occurrence. Meanwhile, the strength reduction with increasing confining pressure is well predicted. Besides, regardless of complicated mechanical process, some other complex features of particle crushing are not considered by this simple model.

4. Elasto-plastic constitutive tensor for model considering particle crushing

To integrate this constitutive model with the finite element analysis, the elasto-plastic constitutive tensor for the proposed model is derived here. The relationship between the elastic stress and strain is expressed in the incrementally linear form as

$$d\sigma_{ij} = D^e_{ijkl}(d\varepsilon_{kl} - d\varepsilon^p_{kl}) \tag{15}$$

where D^e_{ijkl} is the elastic constitutive tensor. ε_{kl} and ε^p_{kl} are the total strain tensor and its plastic component. The yield function f is the function of the stress tensor and the hardening parameter H shown in Eq. (11). The consistency condition can be expressed by

$$\frac{\partial f}{\partial \sigma_{ij}} d\sigma_{ij} + \frac{\partial f}{\partial H} dH = 0 \tag{16}$$

Substituting Eqs. (1), (12) and (15) into Eq. (16) gives

$$\Lambda = \frac{\dfrac{\partial f}{\partial \sigma_{ij}} D^e_{ijkl} d\varepsilon_{kl}}{X} \tag{17}$$

where

$$X = \frac{M_c^4}{M_f^4} \frac{M_f^4 - \eta^4}{M_c^4 - \eta^4} \frac{\partial f}{\partial \sigma_{ij}} \delta_{ij} + \frac{f}{\sigma_{ij}} D^e_{ijkl} \frac{\partial f}{\partial \sigma_{kl}} \tag{18}$$

Substituting Eqs. (12) and (17) into Eq. (15), we get a general form of the proposed model

$$d\sigma_{ij} = D_{ijkl} d\varepsilon_{kl} \tag{19}$$

where the elasto-plastic constitutive tensor D_{ijkl} is expressed as

$$D_{ijkl} = D^e_{ijkl} - D^e_{ijpq} \frac{\partial f}{\partial \sigma_{pq}} \frac{f}{\sigma_{st}} D^e_{stkl} / X \tag{20}$$

The elastic constitutive tensor of Hooke's law for isotropic elasticity can be written as follows

$$D^e_{ijkl} = L\delta_{ij}\delta_{kl} + G(\delta_{ik}\delta_{jl} + \delta_{il}\delta_{jk}) \tag{21}$$

Substituting the Eq. (21) to Eq. (20)

$$D_{ijkl} = L\delta_{ij}\delta_{kl} + G(\delta_{ik}\delta_{jl} + \delta_{il}\delta_{jk}) - \left(L\frac{\partial f}{\partial \sigma_{pp}}\delta_{ij} + 2G\frac{\partial f}{\partial \sigma_{ij}} \right)\left(L\frac{\partial f}{\partial \sigma_{qq}}\delta_{kl} + 2G\frac{\partial f}{\partial \sigma_{kl}} \right) / X \quad (22)$$

where G and L are Lame's constants. And substitute the expression of elastic modulus E in Eq. (13) into G and L

$$G = \frac{E}{2(1+v)} = \frac{3(1-2v)p_a^m}{2mC_e p^{m-1}(1+v)} \quad (23)$$

$$L = \frac{E}{3(1-2v)} - \frac{2}{3}G = \frac{p_a^m}{mC_e p^{m-1}} - \frac{2}{3}G \quad (24)$$

5. Numerical analysis of bearing behavior of model loading pile test

As explained in the model pile loading test, the model pile embedded into uniform Toyoura sand layer was analyzed to clarify its bearing mechanism. Around pile tip area, contraction and distortion of sand accompanying with particle crushing will influence the vertical bearing capacity of model pile to some extent. The particle crushing must be considered to deal with the bearing behavior of sand surrounding the pile tip. The pile is generally modeled as axi-symmetric structure for analytical convenience. The nonlinear finite element analysis incorporating the theory of constitutive model with particle crushing is adopted to improve the accuracy of prediction. The whole analysis area is just the half-structure of the model ground tank container, 300 mm in radius and 550 mm in height. The behavior of Toyoura sand is represented by the constitutive model with particle crushing. The basic physical features of Toyoura sand in triaxial compression test and the ground material in model pile loading tests are the same. Therefore, it is believed that values of the seven parameters are reliable for the numerical analysis of model pile loading test. For calculation simplicity, the meshing work was finished by using basic three nodal triangular elements. The nearer to the pile tip area where complexity distributions of stress, the smaller elements were used. The meshing in the case of model pile with diameter 30mm is shown in Fig. 11. In most recent, numerical analysis of pile loading problem adopting large deformation theory attracts many attentions. It noted that large deformation analysis of pile loading test and remeshing technologies can provide more reliable results and avoid the element distortion in finite element analysis. However, such methods are complicate because that remeshing and adaptive process is intricacy. Nazem *et al*. (2006) compared the predicted pressure under footing using both the large deformation and small deformation analysis. It showed that the discrepancy of predicted pressures between small deformation and large deformation was about 8% when normalized displacement was 0.5. It is acceptable that the finite element analysis of pile loading problem is conducted based on the assumption of small deformation theory in this study.

In accordance with experimental loading approach, displacement-controlled method was also adopted in the numerical computation. The displacement control points are at the bottom of the pile tip and six control points descend simultaneously. The displacement is added by equivalent increment. The final displacement is equal to the pile diameter. Meanwhile, the analytical area of the model ground with the pile diameter of 30 mm is meshed by the same method. The total numbers of the elements and nodes are listed in Table 3.

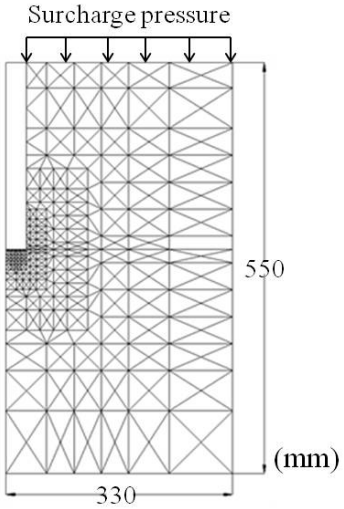

Fig. 11 Element meshing of half-structure of model pile loading test (Diameter = 30 mm)

Table 3 Number of meshing elements and nodes

Model pile diameter	30 mm	54 mm
Total number of elements	873	717
Total number of nodes	473	393

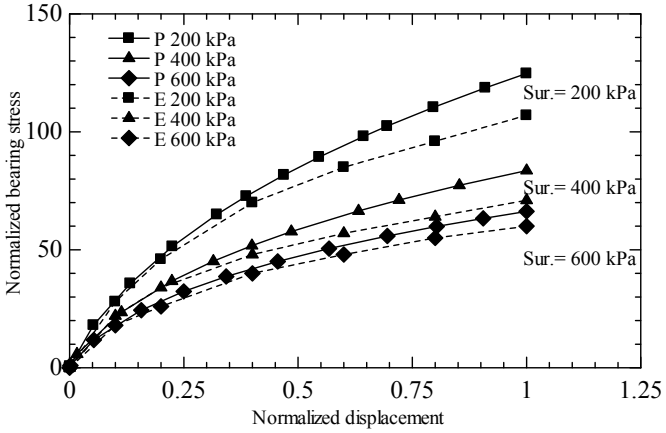

Fig. 12 Relationship between normalized bearing stress and normalized displacement for pile diameter of 30 mm

5.1 Relation between normalized bearing stress and displacement

The numerical and experimental results of the normalized bearing stress and displacement are compared in this study. Herein, the normalized bearing stress is defined by a ratio of current bearing stress of the element beneath pile tip to surcharge pressure acted on the upper surface of

model ground. While the normalized displacement is often adopted in analysis, it is defined as the ratio of current displacement (S) to pile diameter (D). Predicted values by numerical analysis of pile with diameters 30 mm and 54 mm are compared with experimental results in Figs. 12 and 13, respectively. It indicates that the predictions are agreeable with experimental results during the entire loading process under each surcharge pressure. Li and Yamamoto (2005) also attempted to predict the relationship between the normalized bearing stress and displacement of model piles. The predicted result was only agreeable with test results when the normalized displacement was smaller than 0.5. The prediction largely overestimated test result once displacement of pile was larger. The accuracy of prediction is improved by the numerical results incorporating the mechanical characteristics of particle crushing into the constitutive model.

It is interesting to observe that the normalized bearing stress decreases oppositely when the surcharge pressure increase. It can be explained that the amount of sand particles are forced to be crushed under higher surcharge pressure. The reduction of sand strength is attributed to the particle crushing occurrence. It is noticed that all the predicted values slightly overestimate the actual test results as shown in Figs. 12 and 13.

From the comparison of curves between Figs. 8 and 12 or Fig. 13, the same kind of relationship of the normalized bearing stress-displacement can be observed and some further relationship should be researched. In Fig. 8, the vertical axis means the stress ratio of vertical stress to radius stress. The horizontal axis means the axial strain. Similarly in Fig. 12 or Fig. 13, the vertical axis stands for the normalized bearing stress in Fig. 12. The horizontal axis means the normalized displacement with the same expression of axial strain. These two normalized bearing stress-displacement curves are identical in nature. Once the confining stress increases, the normalized bearing stress decreases on the contrary. The deceasing tendency of the normalized bearing stress is related to the particle crushing. It is satisfactory that the predicted values are close to the experiential results during the entire loading process. It is obvious that the pile with larger diameter 54 mm owns much larger bearing stress. It is clear that the interior surface of the ground tank whose size is fixed will provide higher resistance when the diameter of pile becomes larger.

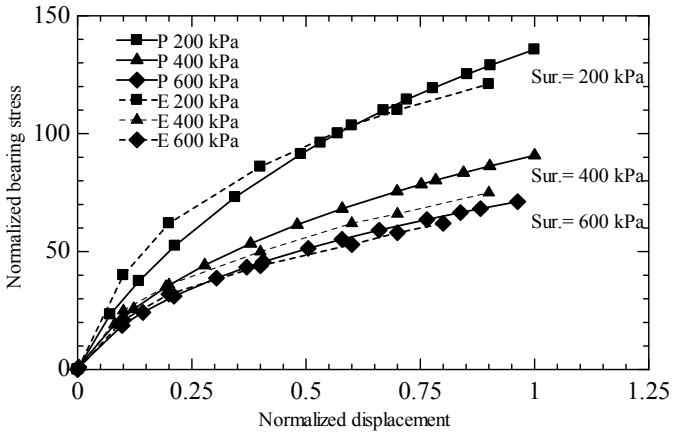

Fig. 13 Relationship between normalized bearing stress and normalized displacement for pile diameter of 54 mm

5.2 *Stress and strain distribution around the pile tip*

Sometimes, the bearing capacity of the pile is not enough to understand soil behavior surrounding pile tip. The distributions and developments of stress and strain quantities around pile tip are significant to achieve such goal. The visualized distributions of stress and strain are beneficial to comprehend soil behavior around pile intuitively. To display the distribution clearly, distributed region is defined not the whole analytical area but only the area in surrounding of the pile tip 216 mm in height and 108 mm in radius corresponding to the model pile loading tests.

Developments of stress and stain quantity variant tendency with surcharge pressure level are discussed from Fig. 14 to Fig. 16. In which, each figure is composed of four sub-titles. The mean stress and deviatoric stress are shown in figures (a) and (b). Plastic volumetric and deviatoric strain indicating the crushing and sliding of particles are vividly depicted in figures (c) and (d). It is estimated that the mean stress p is derived to enhance by model pile embedded deeper in the model ground container and larger surcharge pressure. The distributions of the mean stress under three kinds of surcharge pressures are compared among Figs. 14(a), 15(a) and 16(a). It clearly shows that high mean stress is concentrated in the soil element beneath pile tip. The distributed areas of the high mean stress p and deviatoric stress q expand as surcharge pressure increases. The distribution of mean stress becomes wider in radial and downward direction. The value of the mean stress decreases with the larger distance between the position of element and pile tip. The distributed shape seems as ellipses and accords with the analytical results from Dijkstra *et al*.

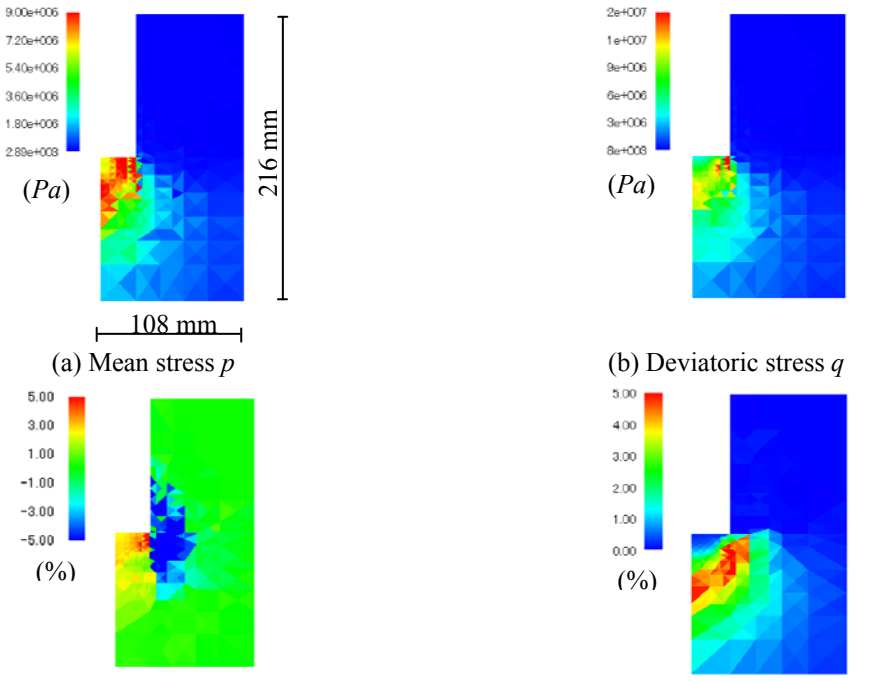

(a) Mean stress p (b) Deviatoric stress q

(c) Plastic volumetric strain ε_v^p (d) Plastic deviatoric strain ε_d^p

Fig. 14 Distributions of stress and strain around pile tip with 30 mm diameter (Surcharge pressure = 200 kPa, S/D = 0.5)

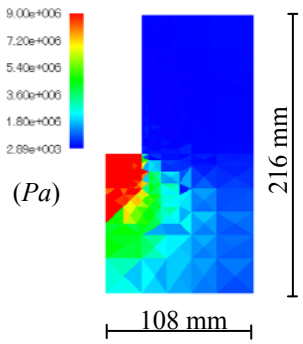

(a) Mean stress p

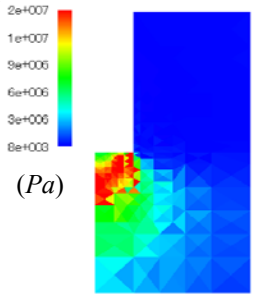

(b) Deviatoric stress q

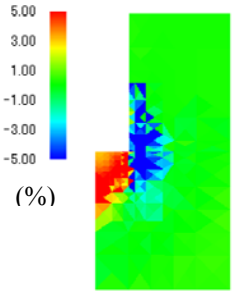

(c) Plastic volumetric strain ε_v^p

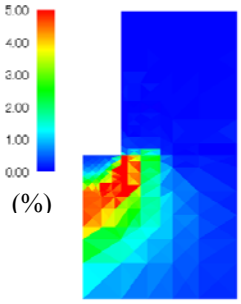

(d) Plastic deviatoric strain ε_d^p

Fig. 15 Distributions of stress and strain around pile tip with 30 mm diameter (Surcharge pressure = 400 kPa, S/D = 0.5)

(2011). In the successive figures of Figs. 14(b), 15(b) and 16(b), distribution of the deviatoric stress under pile tip also amplifies with surcharge pressure's increasing. High-level deviatoric stress firstly appears at the edge of pile tip and shear band is formed. The area of high-level deviatoric stress becomes wider with surcharge pressure's enhancing. It is concluded that the area surrounding the pile tip is subject to significantly complex compression and shear stress.

The predicted vertical stress of element beneath the model pile tip is approximately 20 MPa which is enough to cause Toyoura sand to be crushed. The predicted stress agrees well with the results of model pile loading test performed by Kuwajima *et al*. (2009).

Plastic deformation can be regarded as the total deformation for sand around pile tip because elastic part is negligible compared with plastic part when the deformation of sand is large enough. Among the comparisons of distributions in Figs. 14(c), 15(c) and 16(c), it is predicted that the distributed area of compression is beneath the pile tip. The distributed area of compression forms the wedge. The distributed area and scale of the compression expand with the increasing surcharge pressure and displacement in down direction. The length of the distributed wedge in Fig. 17(c) is almost twice of that in Fig. 15(c) in down direction. The volume contraction of soil beneath pile tip is resulted from the particles crushing and arrangement. Lobo-Guerrero *et al*. (2005, 2007) also predicted that particles crushing are mainly concentrated just beneath pile tip by discrete element method.

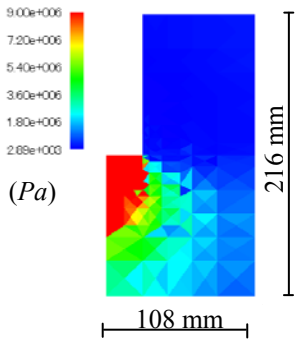

(a) Mean stress p

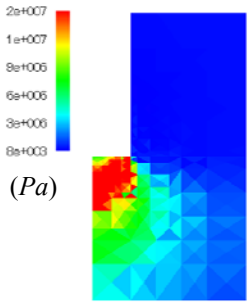

(b) Deviatoric stress q

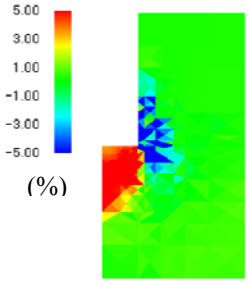

(c) Plastic volumetric strain ε_v^p

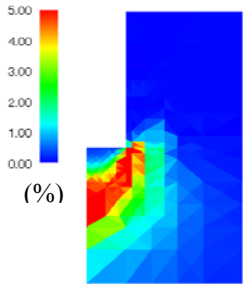

(d) Plastic deviatoric strain ε_d^p

Fig. 16 Distributions of stress and strain around pile tip with 30 mm diameter (Surcharge pressure = 600 kPa, S/D = 0.5)

In addition, the area of the predicted volumetric expansion appears near the pile shaft because the sand particles are highly rotated and sheared. It is observed that the area of distributed expansion slightly contracts with larger surcharge pressure from the Figs. 14(c), 15(c) and 16(c). The disappearance of the expansion should be attributed into the crushing and rearrangement of particles. However, the amount of particle crushing cannot be estimated quantitatively. Under the same surcharge pressure, the distributed shape of expansion shows almost no diffidence when the displacement is large among Figs. 15(c) and 17(c). It is also found by Dijkstra *et al*. (2006) in the similar numerical analysis. The shape of the volumetric expansion amplifies when the surcharge pressure increases from 200 kPa to 400 kPa due to positive dilatancy under the shear stress. But it shrinks when the surcharge pressure is enhanced to 600 kPa.

All the distributions of the plastic deviatoric strain in figure (d) share the same tendency with these of deviatoric stress. The remarkable band indicating high-level shear stress is also formed. The dilatancy behavior of soil around model pile is reasonably predicted and clarified.

The variant of the distribution tendency with the displacement of model pile is discussed in Figs. 15 and 17. In Fig. 15, the displacement ratio is set as $S/D = 0.5$. While it is equal to 1.0 in Fig. 17, the distributions of the mean and deviatoric stresses together with volumetric and deviatoric strain expand with larger displacement. The characteristics of the distribution figures are almost the same.

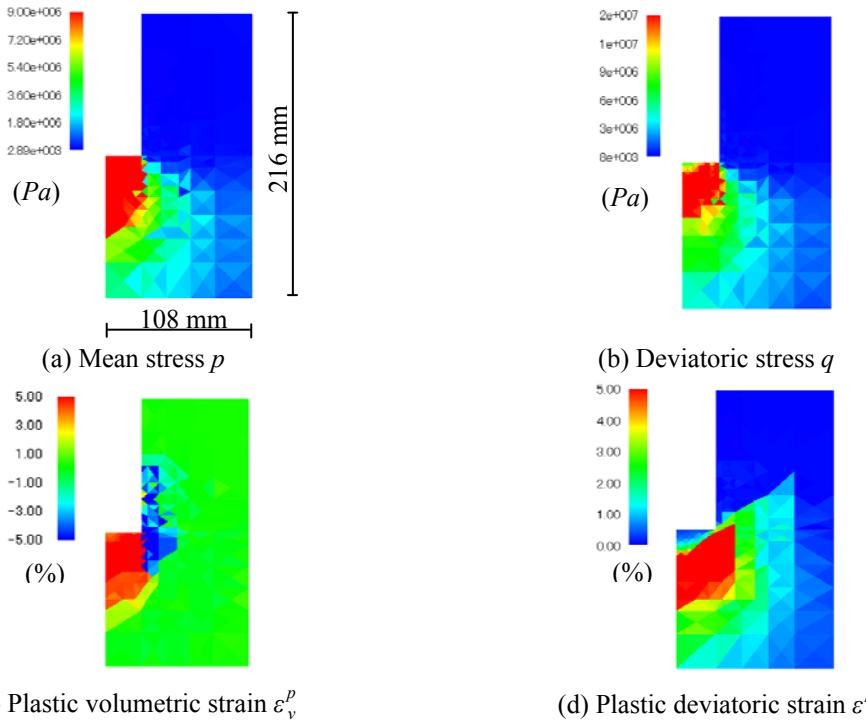

(a) Mean stress p (b) Deviatoric stress q

(c) Plastic volumetric strain ε_v^p (d) Plastic deviatoric strain ε_d^p

Fig. 17 Distributions of stress and strain around pile tip with 30 mm diameter (Surcharge pressure = 400 kPa, S/D = 1.0)

6. Conclusions

In this paper, the importance of the particle crushing in geotechnical problem especially in the pile bearing mechanism is emphasized. A simple constitutive model proposed by Yao *et al.* (2008b) is introduced into finite element method which takes the particle crushing into consideration. The model with particle crushing is also utilized to simulate the soil behavior surrounding the pile tip area where significant stress exits. The analytical program is implemented by displacement- controlled method for more precisely predicted results. It is encouraging that the predicted values are well agreeable with experimental results during the entire loading process. It is further observed that the normalized bearing stress decreases on the contrary although the surcharge pressure is enhanced. It is identical in nature that the normalized bearing stress of triaxial compression test and model pile loading test decreases when confining pressure is enhanced. Both can be explained by the effect of the particle crushing. Simultaneously, the pile with 54 mm diameter has relative larger bearing stress than that of the pile with 30 mm diameter. This can be explained that the resistance pressure provided by interior surface of sand tank with the same size is much larger. It is concluded that the crushing model integrating into the finite element method is an effective method to estimate the bearing capacity of pile.

The developments of the stress and strain around pile tip under different surcharge pressures and penetrating depths are also depicted. The high compressive and sheared region can clarified based on the above analysis. Some conclusions about the distributions can be summarized as

follows. The distribution of the stress value expands with larger surcharge stress and displacement. The distributed shape of the mean stress is ellipse and becomes wider with larger surcharge pressure and displacement. The distributed shape of the deviatoric stress appears firstly near the edge of pile tip and forms the shear band. The volumetric contraction (negative dilatancy) is beneath the pile tip. The area of the predicted compression forms wedge and expands with larger surcharge pressure and displacement in down direction. The area of the predicted volumetric expansion (positive dilitancy) appears near the pile shaft because the sand particles are highly rotated and sheared. With increasing the surcharge pressure, the volumetric expansion slightly compacts because of the crushing and rearrangement of particles. The dilatancy variance can be reasonably described.

The distributed shape of the deviatoric strain shows the same tendency as the deviatoric stress. The remarkable band indicating high-level shear stress is also formed. The developments of stress and strain around pile tip help us to understand the bearing mechanism of pile.

The numerical analysis presented in this paper can be improved by some aspect. For example, finite element analysis with large deformation theory can simulate the actual behavior better. The predicted precision from large deformation theory is believed to be more close to actual solution results with increasing the pile penetration depth. Large deformation theory should be considered and employed for numerical calculation of pile loading or penetrating process in the further work.

References

Daouadji, A., Hicher, P.Y. and Rahma, A. (2001), "An elastoplastic model for granular materials taking into account grain breakage", *Eur. J. Mech. A-Solid.*, **20**(1), 113-137.

Daouadji, A. and Hicher, P.Y. (2010), "An enhanced constitutive model for crushable granular materials", *Int. J. Numer. Anal. Meth. Geomech.*, **34**(6), 555-580.

Dijkstra, J., Broere, W. and Heeres, O.M. (2011), "Numerical simulation of pile intallation", *Comput. Geotech.*, **38**(5),612-622.

Dijkstra, J., Broere, W. and Van, A.F. (2006), "Numerical investigation into stress and strain development around a displacement pile in sand", *Proceedings of the Sixth European Conference on Numerical Methods in Geotechnical Engineering*, Graz, Austria, September, 595-600.

Fukumoto, T. (1992), "Particle breakage characteristics of granular soils", *Soils Found.*, **32**(1), 26-40.

Hardin, B.O. (1985), "Crushing of soil particles", *J. Geotech. Geoenviron. Eng.*, **111**(10), 1177-1192.

Kikumoto, M., Wood, D.M. and Russell, A. (2010), "Particle crushing and deformation behaviour", *Soils Found.*, **50**(4), 547-563.

Kuwajima, K., Hyodo, M. and Hyde, A.F.L. (2009), "Pile bearing capacity factors and soil crushability", *J. Geotech. Geoenviron. Eng.*, **135**(7), 901-913

Lade, P.V., Yamamuro, J.A. and Bopp, P.A. (1996), "Significance of particle crushing in granular materials", *J. Geotech. Geoenviron. Eng.*, **122**(4), 309-316.

Li, W. and Yamamoto, H. (2005), "Numerical analysis on soil behavior around pile-tip under vertical load", *J. Struct. Eng.*, **51**(B), 147-157. [In Japanese]

Lobo-Guerrero, S. and Vallejo, L.E. (2005), "DEM analysis of crushing around driven piles in granular materials", *Geotechnique*, **55**(8), 617-623.

Lobo-Guerrero, S. and Vallejo, L.E. (2007), "Influence of pile shape and pile interaction on the crushable behavior of granular materials around driven piles: DEM analyses", *Granu. Matter.*, **9**(3-4), 241-250.

Mahmound, H., Hosein, S. and Habib, S. (2008), "Dilation and particle breakage effects on the shear strength of calcareous sands based on energy aspects", *Int. J. Civ. Eng.*, **6**(2), 108-117.

Miura, N. and Yamanouchi, T. (1971), "Drained shear characteristics of standard sand under high confining pressures", *Proceedings of Japan Society of Civil Engineering*, **193**, 69-79. [In Japanese]

Miura, N., Murata, H. and Yasufuku, N. (1984), "Stress-strain characteristics of sand in a particle-crushing region", *Soils Found*., **24**(1), 77-89.
Nakai, T. (1989), "An isotropic hardening elastoplastic model for sand considering the stress path dependency in three-dimensional stresses", *Soils Found*., **29**(1), 119-137.
Nazem, M., Sheng, D.C. and Carter, J.P. (2006), "Stress integration and mesh refinement for large deformation in geomechanics", *Int*. *J*. *Numer*. *Meth*. *Engng*, **65**(7), 1002-1027.
Simonini, P. (1996), "Analysis of behavior of sand surrounding pile tips", *J*. *Geotech*. *Geoenviron*. *Eng*., **122**(11), 897-905.
Sun, D.A., Huang, W.X., Sheng, D.C. and Yamamoto, H. (2007), "An elastoplastic model for granular meterials exhibiting particle crushing", *Key Eng*. *Mater*., **340-341**, 1273-1278.
Yamamoto, H., Li, W., Tominaga, K. and Ogura, H. (2003), "Experimental study on effects of overburdening pressures and end shapes for point bearing capacities of pile", *J*. *Struct*. *Eng*., **49**(B), 157-162. [In Japanese]
Yao, Y.P., Sun, D.A. and Matsuoka, H. (2008a), "A unified constitutive model for both clay and sand with hardening parameter independent on stress path", *Comput*. *Geotech*., **35**(2), 210-222.
Yao, Y.P., Yamamoto, H. and Wang, N.D. (2008b), "Constitutive model considering sand crushing", *Soils Found*., **48**(4), 603-608.
Yasufuku, N. and Hyde, A.F.L. (1995), "Pile end-bearing capacity in crushable sands", *Geotechnique*, **45**(4), 663-676.
Yasufuku, N., Ochiai, H. and Ohno, S. (2001), "Pile end-bearing capacity of sand related to soil compressibility", *Soils Found*., **41**(4), 59-71.

CC